

## ORIGINAL ARTICLE

# A mouse model of a human congenital disorder of glycosylation caused by loss of PMM2

Barden Chan<sup>1</sup>, Michelle Clasquin<sup>1</sup>, Gromoslaw A. Smolen<sup>1</sup>, Gavin Histen<sup>1</sup>, Josh Powe<sup>1</sup>, Yue Chen<sup>1</sup>, Zhizhong Lin<sup>2</sup>, Chenming Lu<sup>3</sup>, Yan Liu<sup>3</sup>, Yong Cang<sup>3,4</sup>, Zhonghua Yan<sup>5</sup>, Yuanfeng Xia<sup>5</sup>, Ryan Thompson<sup>6</sup>, Chris Singleton<sup>1</sup>, Marion Dorsch<sup>1</sup>, Lee Silverman<sup>1</sup>, Shin-San Michael Su<sup>1</sup>, Hudson H. Freeze<sup>7</sup> and Shengfang Jin<sup>1,\*</sup>

<sup>1</sup>Agios Pharmaceuticals, Inc., Cambridge, MA 02139-4169, USA, <sup>2</sup>Cancer Research Center, Medical College, Xiamen University, Xiamen 361102, China, <sup>3</sup>WuXi AppTec Co., Ltd, Shanghai 200131, China, <sup>4</sup>Life Sciences Institute and Innovation Center for Cell Signaling Network, Zhejiang University, Hangzhou, Zhejiang 310058, China, <sup>5</sup>HD Biosciences Co., Ltd, Shanghai 201201, China, <sup>6</sup>LGC Genomics, Beverly, MA 01915, USA and <sup>7</sup>Human Genetics Program, Sanford Burnham Prebys Medical Discovery Institute, La Jolla, CA 92037, USA

\*To whom correspondence should be addressed at: Agios Pharmaceuticals, Inc., 88 Sidney Street, Cambridge, MA 02139-4169, USA. Tel: +1 6176498606; Fax: +1 6176498618; Email: Shengfang.Jin@agios.com

## Abstract

The most common congenital disorder of glycosylation (CDG), phosphomannomutase 2 (PMM2)-CDG, is caused by mutations in PMM2 that limit availability of mannose precursors required for protein N-glycosylation. The disorder has no therapy and there are no models to test new treatments. We generated compound heterozygous mice with the R137H and F115L mutations in *Pmm2* that correspond to the most prevalent alleles found in patients with PMM2-CDG. Many *Pmm2*<sup>R137H/F115L</sup> mice died prenatally, while survivors had significantly stunted growth. These animals and cells derived from them showed protein glycosylation deficiencies similar to those found in patients with PMM2-CDG. Growth-related glycoproteins insulin-like growth factor (IGF) 1, IGF binding protein-3 and acid-labile subunit, along with antithrombin III, were all deficient in *Pmm2*<sup>R137H/F115L</sup> mice, but their levels in heterozygous mice were comparable to wild-type (WT) littermates. These imbalances, resulting from defective glycosylation, are likely the cause of the stunted growth seen both in our model and in PMM2-CDG patients. Both *Pmm2*<sup>R137H/F115L</sup> mouse and PMM2-CDG patient-derived fibroblasts displayed reductions in PMM activity, guanosine diphosphate mannose, lipid-linked oligosaccharide precursor and total cellular protein glycosylation, along with hypoglycosylation of a new endogenous biomarker, glycoprotein 130 (gp130). Over-expression of WT-PMM2 in patient-derived fibroblasts rescued all these defects, showing that restoration of mutant PMM2 activity is a viable therapeutic strategy. This functional mouse model of PMM2-CDG, *in vitro* assays and identification of the novel gp130 biomarker all shed light on the human disease, and moreover, provide the essential tools to test potential therapeutics for this untreatable disease.

Received: January 19, 2016. Revised: March 4, 2016. Accepted: March 11, 2016

© The Author 2016. Published by Oxford University Press.

This is an Open Access article distributed under the terms of the Creative Commons Attribution Non-Commercial License (<http://creativecommons.org/licenses/by-nc/4.0/>), which permits non-commercial re-use, distribution, and reproduction in any medium, provided the original work is properly cited. For commercial re-use, please contact [journals.permissions@oup.com](mailto:journals.permissions@oup.com)

**Table 1.** *Pmm2*<sup>R137H/F115L</sup> genotype caused embryonic lethality at > 12.5 dpc, which was not reversed by mannose supplementation

Mannose administered to dams	Gestational stage	Litters, n	Total events, n	WT/WT	R137H/WT	R137H/F115L	P-value compared with expected distribution	
				pups, n (%)	or F115L/WT pups, n (%)	pups, n (%)		
				Expected frequency				
				25%	50%	25%		
No	Term	80	600	177 (29.5)	366 (61.0)	57 (9.5)	<0.0001	
Yes	Term	26	195	53 (27.2)	127 (65.1)	15 (7.7)	<0.0001	
No	12.5 dpc	15	101	27 (26.7)	51 (50.5)	23 (22.8)	0.8493	
No	9.5 dpc	14	117	29 (24.8)	62 (53.0)	26 (22.2)	0.7510	

Expected frequency is based on Mendelian genetics. In the mannose treatment groups, females were administered 9 mg/ml mannose in drinking water for 1 week prior to mating. Mannose treatment continued during pregnancy and halted after pups were born. P-values generated using chi-square test against expected Mendelian distribution.

## Introduction

Congenital disorders of glycosylation (CDG) are rare genetic diseases in which glycosylation pathways are defective (1). Phosphomannomutase 2 (PMM2)-CDG (previously known as CDG-Ia, OMIM Entry No. 212065) is the most commonly diagnosed type and is caused by loss-of-function mutations in PMM2 (2–4). PMM2 is an indispensable enzyme that catalyzes an early step of the N-glycosylation pathway by converting mannose-6-phosphate (M6P) to mannose-1-phosphate (M1P), which is the precursor of guanosine diphosphate mannose (GDP-mannose), and is necessary for the production of dolichol-linked oligosaccharides (DLOs) and a myriad of N-glycans (Supplementary Material, Fig. S1) (1,3,5). Thus, deficiency in PMM2 enzymatic activity causes N-linked hypoglycosylation of proteins. Patients with PMM2-CDG exhibit a wide range of symptoms that can include strabismus, developmental delay, failure to thrive, ataxia, susceptibility to infections, coagulopathy and an increased rate of childhood mortality (3,4,6–10). There is currently no cure or approved treatment for PMM2-CDG. Moreover, no viable mouse model is available for preclinical testing of potential therapeutics.

Here, we report the generation of the first viable *Pmm2* hypomorphic mouse model. The mutant mice carry mutations (R137H and F115L) in the highly conserved PMM2 protein that correspond to the two most prevalent mutations in patients with PMM2-CDG, R141H (NM\_000303.2:c.422G > A (p.Arg141His) ClinVar 7706) and F119L (NM\_000303.2:c.357C > A (p.Phe119Leu) ClinVar 7711). This novel mouse model recapitulates many disease features seen in patients with PMM2-CDG. Using a panel of *in vitro* assays, we confirmed the deficiency in the N-glycosylation pathway in mouse embryonic fibroblasts (MEFs) from *Pmm2*<sup>R137H/F115L</sup> mutants and showed it was consistent with the deficiency in fibroblasts from patients with PMM2-CDG. We also identified a novel cellular glycosylation biomarker, glycoprotein 130 (gp130). Our mouse model, novel biomarker and cell-based assays provide a platform to study the molecular pathobiology of PMM2-CDG.

## Results

### Generation of a hypomorphic PMM2-CDG mouse model that mimics the human disease phenotype

We aimed to create a viable hypomorphic mouse model of PMM2-CDG. Previous reports showed that *Pmm2* null mice die very early in embryogenesis (11) and mice of a hypomorphic

line (*Pmm2*<sup>R137H/F118L</sup>) die by mid-gestation (12). We created a hypomorphic mouse line that harbored the *Pmm2*<sup>R137H/F115L</sup> compound heterozygous mutations (Supplementary Material, Fig. S2), which is equivalent to the most common genotype (*PMM2*<sup>R141H/F119L</sup>) found in human patients with PMM2-CDG (Supplementary Material, Fig. S3) (2,13–17). Our model is distinct from a previously described *Pmm2* mouse model (*Pmm2*<sup>R137H/F118L</sup>), in which the F118L mutation is equivalent to a synthetic mutation F122L in the human PMM2 protein (12). Homozygous *Pmm2*<sup>R137H/R137H</sup> embryos showed complete embryonic lethality, which is consistent with homozygous *PMM2*<sup>R141H/R141H</sup> mutations never being observed in human PMM2-CDG (18). Significant embryonic lethality also occurred in our *Pmm2*<sup>R137H/F115L</sup> population at > 12.5 days post coitum (dpc) (Table 1). In the previous *Pmm2*<sup>R137H/F118L</sup> model, Schneider et al. (12) showed that providing mannose (9 mg/ml) in the drinking water of dams rescued embryonic lethality. The authors suggested that exogenous mannose increases the metabolic flux of mannose into the pathway and overcomes the reduced PMM2 activity caused by R137H and F118L mutations. Providing our dams with the same amount of mannose did not rescue embryonic lethality in *Pmm2*<sup>R137H/F115L</sup> pups (Table 1); however, this amount of mannose significantly rescued embryonic lethality in *Pmm2*<sup>F115L/F115L</sup> homozygous mutants (Table 2). We attempted to identify prenatal gross organ defects in *Pmm2*<sup>R137H/F115L</sup> mutant mice by histological examination of surviving embryos at 16.5 dpc; however, no significant genotype-specific histological changes in mutant versus wild-type (WT) embryos were observed at this developmental stage (data not shown).

Our *Pmm2* hypomorphic model yields viable *Pmm2*<sup>R137H/F115L</sup> offspring for postnatal studies, enabling comparison with the clinical and molecular features of patients with PMM2-CDG. We observed significant postnatal death in *Pmm2*<sup>R137H/F115L</sup> mice (50.9% survival at postnatal Day 65) while survival of heterozygous pups was similar to WT siblings (98.9% and 100% survival at Day 65, respectively, Fig. 1A). All *Pmm2*<sup>R137H/F115L</sup> mutant mice were visibly smaller than their littermates (Supplementary Material, Fig. S4A) and displayed lower body weight versus WT or heterozygous *Pmm2*<sup>R137H/WT</sup> and *Pmm2*<sup>F115L/WT</sup> littermates (Fig. 1B and C). We also observed that 3 of 31 (10%) *Pmm2*<sup>R137H/F115L</sup> mice exhibited various ocular anomalies, including appearance of secretions and inability to open the eye (Supplementary Material, Fig. S4B) and 2 of 31 (6%) mice displayed hind leg hypotonia (Supplementary Material, Fig. S4C). Multiple (9 of 31; 29%) *Pmm2*<sup>R137H/F115L</sup> mice also had various degrees of kyphosis (Supplementary Material, Fig. S4D), a disease feature documented in patients with PMM2-CDG (6,8,9). Two-dimensional

**Table 2** *Pmm2*<sup>F115L/F115L</sup> genotype caused embryonic lethality that could be reversed by mannose supplementation

Mannose administered to dams	Gestational stage	Litters, n	Total events, n	WT/WT pups, n (%)	F115L/WT pups, n (%)	F115L/F115L pups, n (%)	P-value compared with expected distribution			
								Expected frequency		
								25%	50%	25%
No	Term	10	82	23 (28.1)	51 (62.2)	8 (9.75)	0.0056			
Yes	Term	16	111	31 (27.9)	57 (51.4)	23 (20.72)	0.5395			
No	12.5 dpc	18	132	38 (28.8)	63 (47.7)	31 (24.48)	0.6020			
No	9.5 dpc	7	58	14 (24.1)	33 (56.9)	11 (18.97)	0.4932			

Expected frequency is based on Mendelian genetics. In the mannose treatment group, females were treated with 9 mg/ml mannose in drinking water for 1 week prior to mating. Mannose treatment continued during pregnancy and halted after pups were born. P-values generated using chi-square test against expected Mendelian distribution.

(2D) micro-computed tomography (CT) imaging revealed a more pronounced curvature of the spine in *Pmm2*<sup>R137H/F115L</sup> mice compared with WT (Supplementary Material, Fig. S4E). 3D micro-CT scans further detailed the abnormal skeletal features seen in *Pmm2*<sup>R137H/F115L</sup> mice, which included kyphosis, failed closure of the posterior fontanelle (the lower bone at the back of the skull) and defective development of the cervical spine near the base of the skull (Supplementary Material, Fig. S5).

Next, we performed histological examination of three pairs of sex-matched WT and *Pmm2*<sup>R137H/F115L</sup> mice at 4 weeks of age. Mild myocardial atrophy characterized by decreased thickness of both left and right ventricular walls and the interventricular septum, and decreased width of individual myofibers were observed in all three *Pmm2*<sup>R137H/F115L</sup> mice examined (Fig. 2A and B; Supplementary Material, Table S1). In the liver, we detected hepatocellular eosinophilic cytoplasmic hyaline bodies in *Pmm2*<sup>R137H/F115L</sup> mice (Fig. 2C). Mild dilation in the proximal tubule was observed consistently in the kidneys of *Pmm2*<sup>R137H/F115L</sup> mice, and was characterized by increased luminal space and loss of definition of the brush border of tubular epithelium (Fig. 2D). Rare degenerate cells were also present within the tubular epithelium or lumen (not shown). In contrast to patients with PMM2-CDG, we did not observe changes in the brain/cerebellum in *Pmm2*<sup>R137H/F115L</sup> mutant mice (Fig. 2E; Supplementary Material, Table S1). Specifically, the density of Purkinje cells in the cerebellar folia did not differ between the two groups. It should be noted that histological examination was only performed on *Pmm2*<sup>R137H/F115L</sup> mutant mice surviving to 4 weeks of age. Abnormal central nervous system pathology could have been present in the more severely affected mutants that died postnatally; however, we were unable to preserve these samples for histology. No histological differences were detected in lungs and spleens between WT and *Pmm2*<sup>R137H/F115L</sup> mice (data not shown).

### ***Pmm2*-mutant mice have dysregulated levels of circulating proteins**

Patients with PMM2-CDG typically have decreased levels of circulating antithrombin III (ATIII), insulin-like growth factor (IGF)-1, IGF binding protein-3 (IGFBP-3) and acid-labile subunit (ALS) (19–21). These plasma proteins were also deficient in *Pmm2*<sup>R137H/F115L</sup> mice when compared with WT mice or heterozygous littermates carrying one of the mutant alleles: ATIII was reduced by 37% ( $P < 0.0001$ ), IGFBP-3 by 41% ( $P < 0.0001$ ) and IGF-1 by 30% ( $P < 0.0001$ ; Fig. 3A). *Pmm2*<sup>R137H/F115L</sup> mice had a nearly complete absence of ALS (Fig. 3B, upper), an IGF-binding protein that is

normally highly N-glycosylated. In contrast to patients with PMM2-CDG (22), plasma transferrin glycosylation was normal in *Pmm2*<sup>R137H/F115L</sup> mice, as measured by western blot (Fig. 3B, lower) and confirmed by additional liquid chromatography-mass spectrometry (LC-MS) protein analysis (data not shown).

To identify novel potential biomarkers in *Pmm2*<sup>R137H/F115L</sup> sera, we tested an array of antibodies against 83 serum proteins from WT and *Pmm2*<sup>R137H/F115L</sup> samples and validated our findings by enzyme-linked immunosorbent assay (ELISA). Two glycoprotein biomarkers, pentraxin 3 (PTX3) and IGFBP-1 were significantly upregulated in *Pmm2*<sup>R137H/F115L</sup> mice (Fig. 3C). N-glycosylated PTX3 was upregulated ~2-fold ( $P \leq 0.0001$ ) in *Pmm2*<sup>R137H/F115L</sup> samples compared with the other genotypes. Strikingly, IGFBP-1, an O-glycosylated protein that binds to IGF-1 but not to ALS (23, 24), was upregulated >13-fold in *Pmm2*<sup>R137H/F115L</sup> mice compared with control WT mice (Fig. 3C).

### ***Pmm2*-mutant fibroblasts are deficient in the PMM2 pathway**

We analyzed MEFs from these mutant embryos and found that PMM2 protein levels in *Pmm2*<sup>R137H/WT</sup> and *Pmm2*<sup>F115L/WT</sup> MEFs were ~50% of levels in WT MEFs, whereas PMM2 levels in *Pmm2*<sup>R137H/F115L</sup> MEFs were ~25–30% that of WT MEFs (Supplementary Material, Fig. S6). *In vitro* total PMM enzymatic activity in *Pmm2*<sup>R137H/WT</sup> and *Pmm2*<sup>F115L/WT</sup> MEFs was ~45–60% of that in WT MEFs, whereas activity in *Pmm2*<sup>R137H/F115L</sup> MEFs was 15–16% of WT PMM2 activity (Fig. 4A). Lower cellular PMM activity also resulted in reductions in mannose-related downstream metabolites, such as GDP-mannose (Fig. 4B) and DLO (Fig. 4C), and in global protein mannosylation (Fig. 4D). Finally, we looked at the glycosylation status of endogenous gp130, a heavily N-glycosylated protein (25). Western blot results showed that WT MEFs expressed full length, fully glycosylated gp130, whereas the *Pmm2*<sup>R137H/F115L</sup> MEFs expressed under-glycosylated gp130 (Fig. 4E).

### **PMM2 pathway activity is diminished in PMM2-CDG patient primary fibroblasts**

To better understand the PMM2 pathway in CDG patients, we tested fibroblasts isolated from 10 patients with different PMM2 genotypes (Supplementary Material, Table S2). Western blots revealed that these fibroblasts expressed less PMM2 protein than PMM2 WT HFF-1 fibroblasts (Fig. 5A). As expected, total PMM activity in these patient fibroblasts was 37–89% lower than

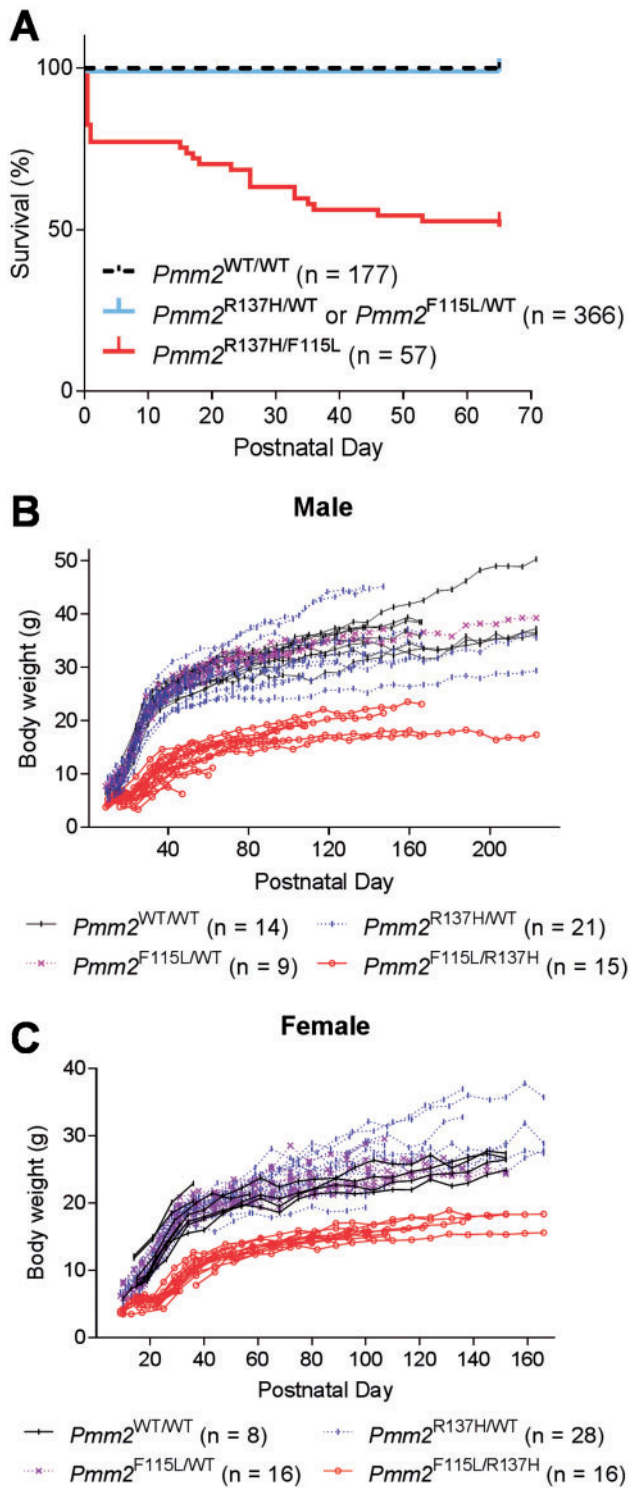


**Figure 1.** Survival and growth of  $Pmm2^{R137H/F115L}$  mice was reduced. (A) 600 pups from 80 matings of  $Pmm2^{R137H/WT}$  and  $Pmm2^{F115L/WT}$  were monitored for postnatal lethality. The  $Pmm2^{R137H/F115L}$  genotype induced postnatal death. The four deaths in the heterozygotes all occurred on postnatal Day 1 due to abandonment of pups by young mothers because the mother was disturbed.  $Pmm2^{R137H/F115L}$  mice demonstrated lower body weight in males (B) and females (C) throughout the period monitored. Only litters with surviving  $Pmm2^{R137H/F115L}$  mice were used to generate B and C.

that of control HFF-1 cells (Fig. 5B). In addition, levels of metabolites downstream of PMM2, such as DLO (Fig. 5C) and GDP-mannose (Fig. 5D), were also reduced in patient cells. All of the CDG patient fibroblasts had a diminished ability to fully mannose proteins *in vitro* (Fig. 5E).

To demonstrate that the overall reduction in pathway activity and mannosylation was specifically due to defective PMM2 activity, we rescued the phenotype by overexpressing WT-PMM2 in patient cells. We used CDG-168 cells since they have the human mutations ( $PMM2^{R141H/F119L}$ ) that correspond to the mutations in our mouse model. As expected, overexpressing WT-PMM2 (Fig. 6A) restored normal intracellular levels of GDP-mannose (Fig. 6B), DLO (Fig. 6C) and global mannosylation (Fig. 6D) in CDG-168 cells.

Next, we investigated whether specific glycoprotein expression was also influenced by PMM2 activity in these patient fibroblasts by western blotting. Using these skin fibroblasts, we were unable to examine the expression of the liver-specific glycoproteins (ATIII, IGF-1 and ALS) that were severely affected by PMM2 mutations in mice. However, we found that expression of glycosylated intercellular adhesion molecule-1 (ICAM-1) induced by tumor necrosis factor- $\alpha$  (TNF $\alpha$ ) was greatly enhanced in CDG-168 fibroblasts when they overexpressed WT-PMM2 (Fig. 6E). In addition, expression of fully glycosylated gp130 and secretion of IGFBP-3 were significantly increased in CDG-168 fibroblasts that overexpressed WT-PMM2, as measured by western blotting and ELISA, respectively (Fig. 6F and G). These data are consistent with our observations that  $Pmm2^{R137H/F115L}$  MEFs from our mouse model expressed significantly less fully glycosylated gp130 compared with WT MEFs, and that plasma IGFBP-3 levels in  $Pmm2^{R137H/F115L}$  mice were significantly lower than in WT mice.

## Discussion

Our main objective was to develop a viable mouse model that mimicked human PMM2-CDG. Previously, Schneider et al. (12) created a  $Pmm2$  hypomorphic mouse model with R137H and F118L mutations which showed complete embryonic lethality of  $Pmm2^{R137H/F118L}$ , and was thus severely limited in its utility. In contrast,  $Pmm2^{F118L/F118L}$  mutants were indistinguishable from WT siblings. Our novel model is unique, since the genotype  $Pmm2^{R137H/F115L}$  is equivalent to the most common mutation in patients with PMM2-CDG,  $PMM2^{R141H/F119L}$ .  $Pmm2^{R137H/F115L}$  mice also showed some embryonic lethality. This partial embryonic lethality could not be rescued by administering mannose to dams, in contrast to the embryonic lethality of the  $Pmm2^{R137H/F118L}$  genotype, which could. This difference may be due to the specific nature of the second  $Pmm2$  mutation. PMM2 with the F119L mutation (equivalent to F115L in mice) displays only 25% of the activity of WT PMM2 (27), whereas PMM2 with the F122L mutation (equivalent to F118L in mice) is expected to display a mild loss of enzymatic activity (12). It might also be due to the different genetic backgrounds of the two strains used, which was a C57Bl6-SV129 mixed background in the current study, and C57Bl6 in the Schneider et al.  $Pmm2^{R137H/F118L}$  mice. Differences in chow and housing could also contribute to the differences between the two studies.

However, a significant number of  $Pmm2^{R137H/F115L}$  offspring survived, and showed many disease features observed clinically in patients with PMM2-CDG. The mortality rate in patients with PMM2-CDG can be as high as 20% in the early years of life (28) but the degree of pre and perinatal lethality is unknown. Our  $Pmm2^{R137H/F115L}$  mice also exhibited a high level of postnatal

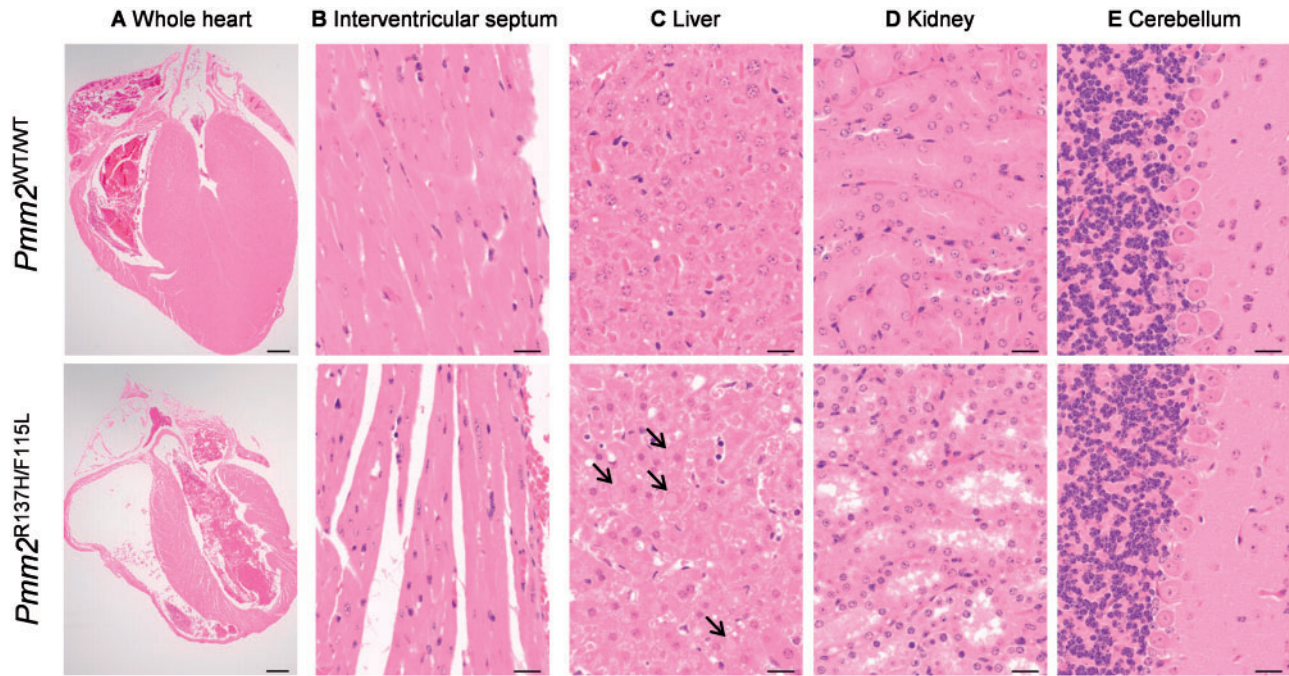


**Figure 2** Surviving *Pmm2*<sup>R137H/F115L</sup> mice showed additional postnatal defects in multiple organ systems. Three pairs of sex-matched 4-week-old *Pmm2*<sup>WT/WT</sup> and *Pmm2*<sup>R137H/F115L</sup> mice were examined. Representative H&E staining of sections from (A) the whole heart (bar = 500  $\mu$ m), (B) interventricular septum, (C) liver, (D) kidney and (E) cerebellum shown (bar = 20  $\mu$ m for B, C, D and E). A and B demonstrate the decreased wall thickness of both ventricles and the interventricular septum, and decreased diameter (amount of cytoplasm) of individual myofibers in *Pmm2*<sup>R137H/F115L</sup> compared with *Pmm2*<sup>WT/WT</sup> mice. C demonstrates the accumulation of cytoplasmic hyaline bodies in the liver of the mutant mice, indicated by arrows. D demonstrates the tubular dilation observed in the kidneys of mutant mice. E illustrates the lack of an effect on the Purkinje cell density in the cerebellum of mutant mice.

mortality. Patients also have significant postnatal growth failure (29), and many have additional symptoms such as kyphosis, ophthalmological problems and axial hypotonia (28). All of our surviving *Pmm2*<sup>R137H/F115L</sup> mutants had stunted growth, while heterozygous mice carrying a single mutation were indistinguishable from WT siblings. A small percentage of *Pmm2*<sup>R137H/F115L</sup> mice exhibited hind leg hypotonia, eye defects and curvature of the spine. Although seen in other CDGs, ocular anomalies are not often seen in PMM2-CDG. The hind leg hypotonia we observed is considered to be a peripheral motor neuropathy, which contrasts with the central hypotonia seen in children with PMM2-CDG. The exact causes of these differences in disease features between mutant mice and human patients are currently unknown. Although the number of individual mice affected with these additional disease features was small, our results nonetheless indicate that this new PMM2-CDG mouse model shows the broad spectrum of heterogeneity of disease presentation that is often seen in patients with PMM2-CDG.

Our *Pmm2*<sup>R137H/F115L</sup> mice also had molecular characteristics typical of patients with PMM2-CDG including reduced levels of IGF-1, IGFBP-3, ALS and ATIII (19–21). Although IGF-1 is not N-glycosylated, its level is 3.2-fold lower in the compound heterozygous mice, presumably due to the loss of its two stabilizing N-glycoproteins, IGFBP-3 and ALS. When IGF-1 is in a ternary complex with IGFBP-3 and ALS, its half-life is 16–20 h (23). The half-life of IGF-1 drops dramatically when it is in unbound form (1–2 min), or when bound only to IGFBP-3 (20–30 min). We speculate that the loss of N-glycosylation of IGFBP-3 and ALS led to decreased protein levels and a subsequent reduction in IGF-1 levels due to its decreased half-life. This imbalance of the IGF system is likely to be the major reason for the growth defects found in the *Pmm2*<sup>R137H/F115L</sup> mutant mice, and growth defects

are the most consistent gross abnormality in patients with PMM2-CDG.

Next, we sought to identify novel circulating PMM2-CDG biomarkers. We found that IGFBP-1 was highly upregulated (>13-fold) in the *Pmm2*<sup>R137H/F115L</sup> mouse population but was nearly undetectable in the *Pmm2*<sup>WT/WT</sup> samples. The IGFBP-1 increase could be due to transcriptional regulation operating via an unknown mechanism to maintain IGF homeostasis. In the PMM2-deficient animals, this increase could be part of a compensatory mechanism that attempts to stabilize IGF-1 upon loss of IGFBP-3 and ALS. We also found that PTX3 was significantly upregulated in the *Pmm2*<sup>R137H/F115L</sup> mouse population compared with WT littermates. PTX3 binds to several members of the complement system and is an important marker for inflammation (30). Despite the fact that PTX3 has a single N-glycosylation site, *Pmm2*<sup>R137H/F115L</sup> mice had elevated levels of circulating PTX3. The exact mechanisms and biological significance of this upregulation are unknown at this point. As with the growth reduction phenotype, these alterations in molecular marker levels were observed in *Pmm2*<sup>R137H/F115L</sup> but not *Pmm2*<sup>R137H/WT</sup> or *Pmm2*<sup>F115L/WT</sup> genotypes.

Transferrin glycosylation status is commonly used as a biomarker for human CDGs (31–34). However, circulating transferrin from *Pmm2*<sup>R137H/F115L</sup> mice did not show hypoglycosylation by western blot. This observation was supported by additional LC-MS protein analysis. Schneider et al. reported normal transferrin glycosylation in their *Pmm2* hypomorphic model (12). Transferrin glycosylation was also normal in mice that have hypomorphic mutations (*Mpi*<sup>Y255C/Y255C</sup>) in phosphomannose isomerase (MPI), and show hypoglycosylation of other proteins (35). Thus, it appears that transferrin is not a reliable hypoglycosylation marker in mice, in contrast to humans.

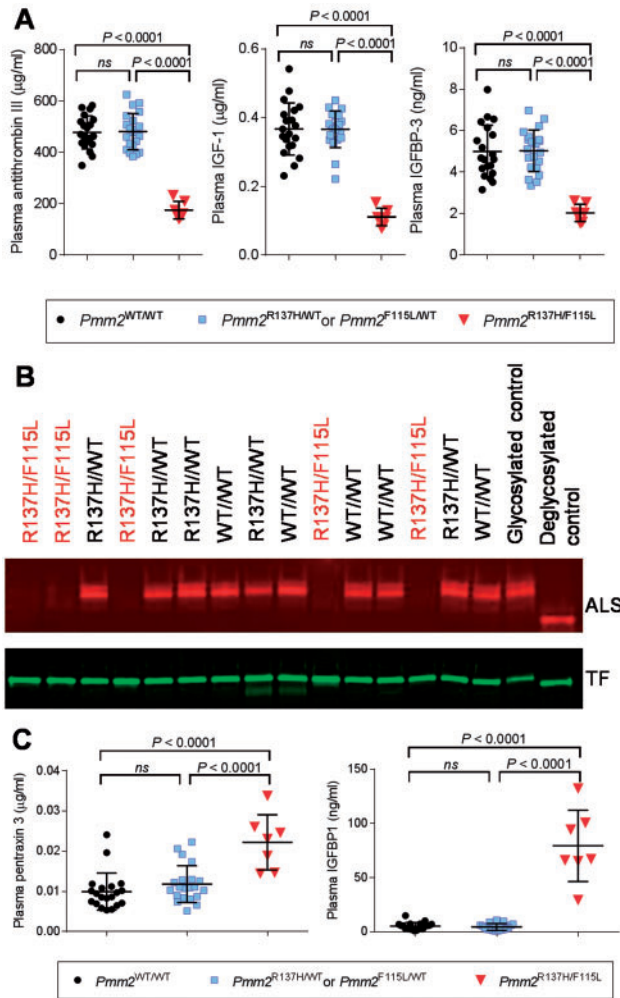


**Figure 3**  $Pmm2^{R137H/F115L}$  mice have significantly altered levels of disease-relevant plasma biomarkers. (A) Mean ( $\pm$ SD) levels of ATIII, IGF-1 and IGFBP-3 measured by ELISA in plasma of  $Pmm2^{WT/WT}$  ( $n=21$ ),  $Pmm2^{R137H/WT}$  or  $Pmm2^{F115L/WT}$  ( $n=20$ ) and  $Pmm2^{R137H/F115L}$  ( $n=7$ ) mice.  $P$ -values were generated using one-way ANOVA test followed by Tukey post-hoc tests for multiple comparisons. (B) Glycosylation and expression level of ALS and transferrin in mouse plasma (genotype indicated above, hypomorphic mutants labeled in red). The two lanes on the far right are controls. Glycosylated control was a sample of normal B6 mouse plasma. Deglycosylated control was a sample of normal B6 mouse plasma de-glycosylated *in vitro* by *N*-glycanase. Note an increase in migration rate for both ALS and transferrin after *N*-glycanase treatment. (C) Mean ( $\pm$ SD) levels of PTX3 and IGFBP-1 measured by ELISA in plasma of  $Pmm2^{WT/WT}$  ( $n=21$ ),  $Pmm2^{R137H/WT}$  or  $Pmm2^{F115L/WT}$  ( $n=20$ ) and  $Pmm2^{R137H/F115L}$  ( $n=7$ ) mice.  $P$ -values were generated using one-way ANOVA test followed by Tukey post-hoc tests for multiple comparisons.

Collectively, our biomarker analysis suggests that IGFBP-3, IGF1, ALS and ATIII could be useful biomarkers in future studies of therapeutic interventions as they are also known to be altered in patients with PMM2-CDG. In addition, IGFBP-1 and gp130 measurements may provide a larger dynamic range for tracking disease normalization by therapeutic interventions in this mouse model, although further validation will be needed to assess their relevance in patients.

Using *in vitro* studies, we also confirmed that metabolic changes in MEFs isolated from  $Pmm2^{R137H/F115L}$  mice were similar to changes observed in fibroblasts isolated from patients with PMM2-CDG. Levels of key metabolites such as GDP-mannose and DLO were significantly reduced in  $Pmm2^{R137H/F115L}$

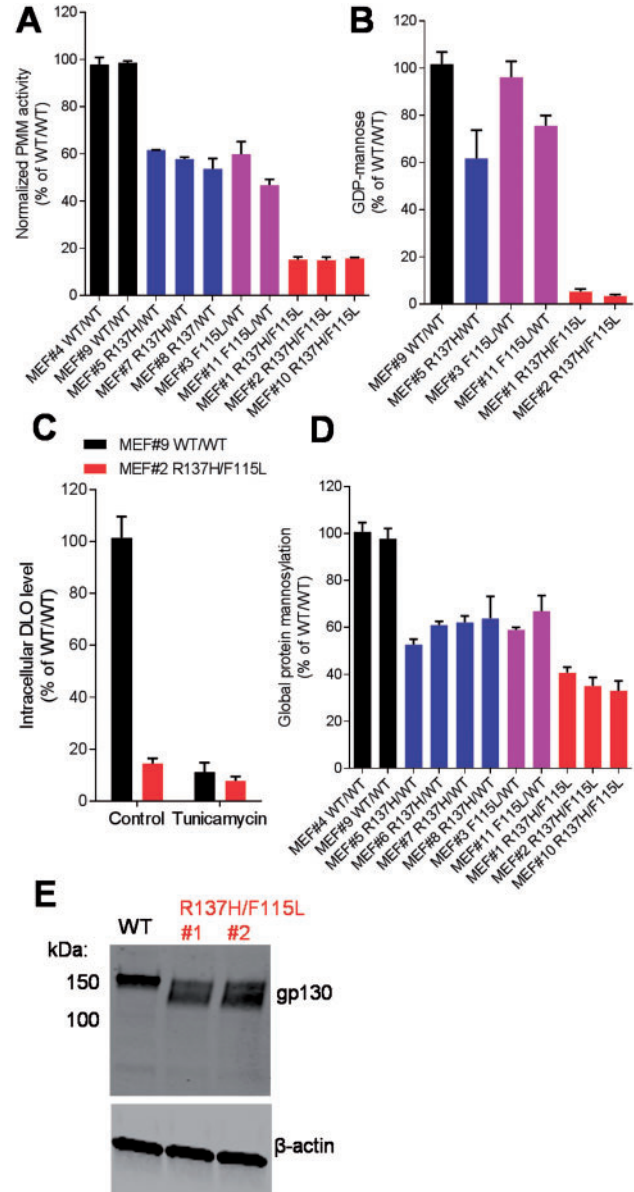


**Figure 4** Mutant  $Pmm2$  knock-in mice have reduced PMM activity. (A) Total PMM enzymatic activity was reduced by  $Pmm2$  R137H and F115L mutations. MEFs isolated from individual mice were numerically labeled. (B) GDP-mannose level was significantly reduced in  $Pmm2^{R137H/F115L}$  MEFs when incubated for 5 h without glucose. This difference was rescued *in vitro* by high glucose concentration (data not shown) as reported previously (26). (C) DLO levels in  $Pmm2^{WT/WT}$  MEFs were significantly lower than that in  $Pmm2^{WT/WT}$ . Levels of endogenous DLO were completely suppressed by addition of tunicamycin at  $10 \mu\text{g/ml}$  overnight prior to harvesting. (D) Global mannosylation was reduced in  $Pmm2$ -mutant MEFs as measured by incorporation of  $^3\text{H}$  mannose into cellular protein fractions. (E) Hypoglycosylation of gp130 was detected in  $Pmm2^{R137H/F115L}$  MEFs as judged by SDS-PAGE migration detected by western blotting. Each experiment was repeated at least twice. In A–D, representative data from one experiment are shown as mean  $\pm$  SD from triplicate.

MEFs, leading to reduction in overall protein mannosylation. Similar metabolic changes were detected *in vitro* in 10 PMM2-CDG fibroblast cell lines with different genotypes. The reduction in, but not complete depletion of, PMM activity we observed in all the CDG patient-derived cells supports the hypothesis that disease alleles are hypomorphic, and that mutations leading to

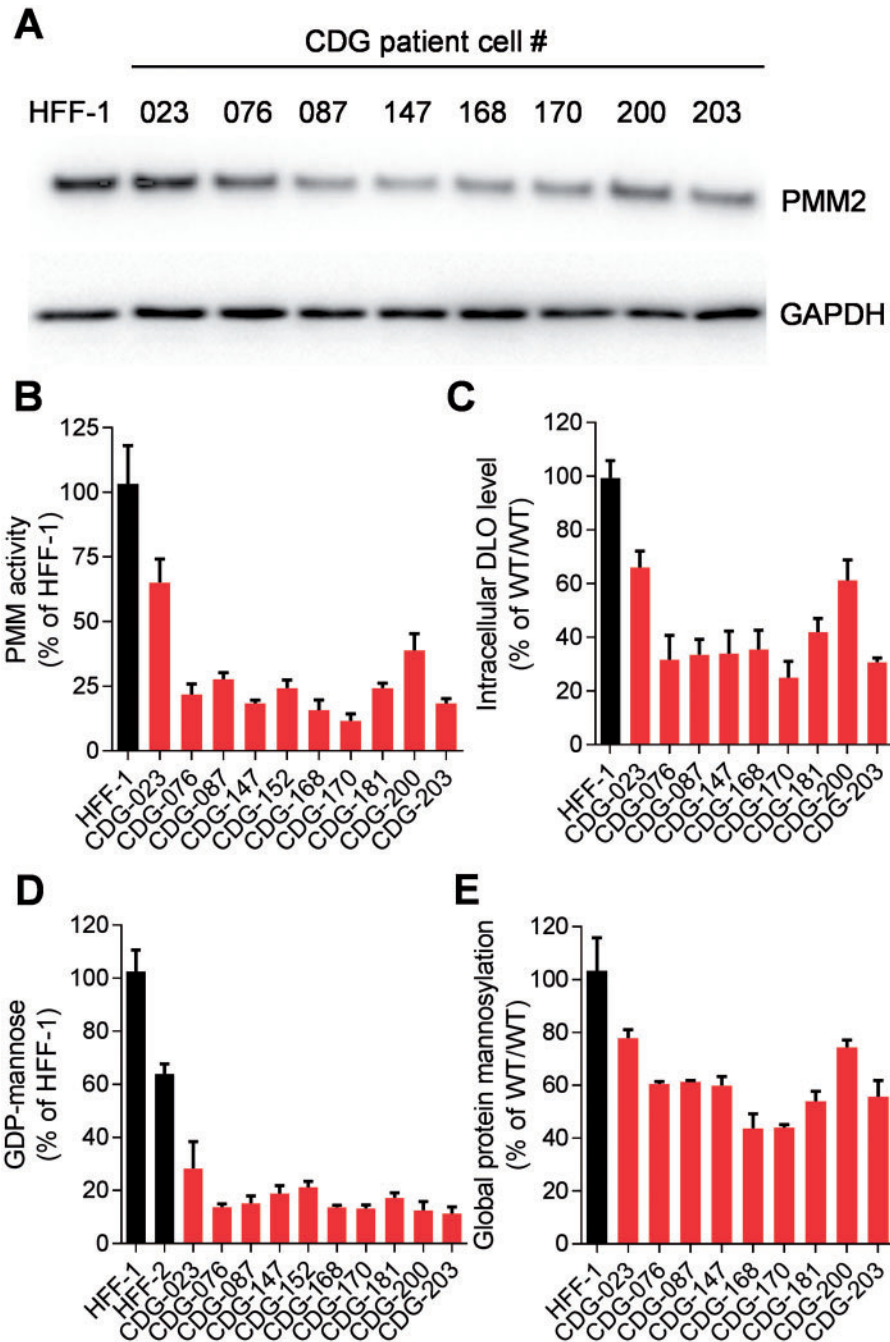


**Figure 5** PMM2 pathway activity characterization of PMM2-CDG patient fibroblasts. (A) Western blot showing lower expression level of PMM2 protein in a panel of PMM2-CDG patient fibroblasts (B) PMM activity was diminished in multiple PMM2-CDG patient fibroblast cell lines with different genotypes compared with normal fibroblasts. Data represent the average of three assays run in quadruplicate and error bars represent SD. (C) DLO levels were reduced in patient fibroblasts. (D) Intracellular levels of GDP-mannose were diminished in multiple PMM2-CDG patient fibroblast cell lines with different genotypes compared with normal fibroblasts, under glucose-free conditions. Data represent the average of three experiments and error bars represent SD. This difference was rescued *in vitro* by high glucose concentration (data not shown) as reported previously (26). (E) Protein mannosylation levels were also reduced in patient fibroblasts. Each experiment was repeated at least twice. Representative data from one experiment are shown as mean  $\pm$  SD from triplicates.

complete loss of PMM2 are lethal [further supported by the early embryonic lethality of *Pmm2* null mice (11)]. As expected, over-expression of WT human PMM2 in patient-derived fibroblasts restored PMM2 pathway metabolite levels and protein mannosylation.

Significantly, we discovered that the glycoprotein gp130 was hypoglycosylated in both *Pmm2*<sup>R137H/F115L</sup> MEFs and

PMM2-CDG patient fibroblasts. Gp130 is a co-receptor for all members of the interleukin-6 (IL-6) receptor family and is required for signal transduction by IL-6-type cytokines (36). Its stability is enhanced by N-glycosylation at nine sites (25). We also noted that primary fibroblasts isolated from other types of CDG had reduced N-glycosylation of gp130 (unpublished results).

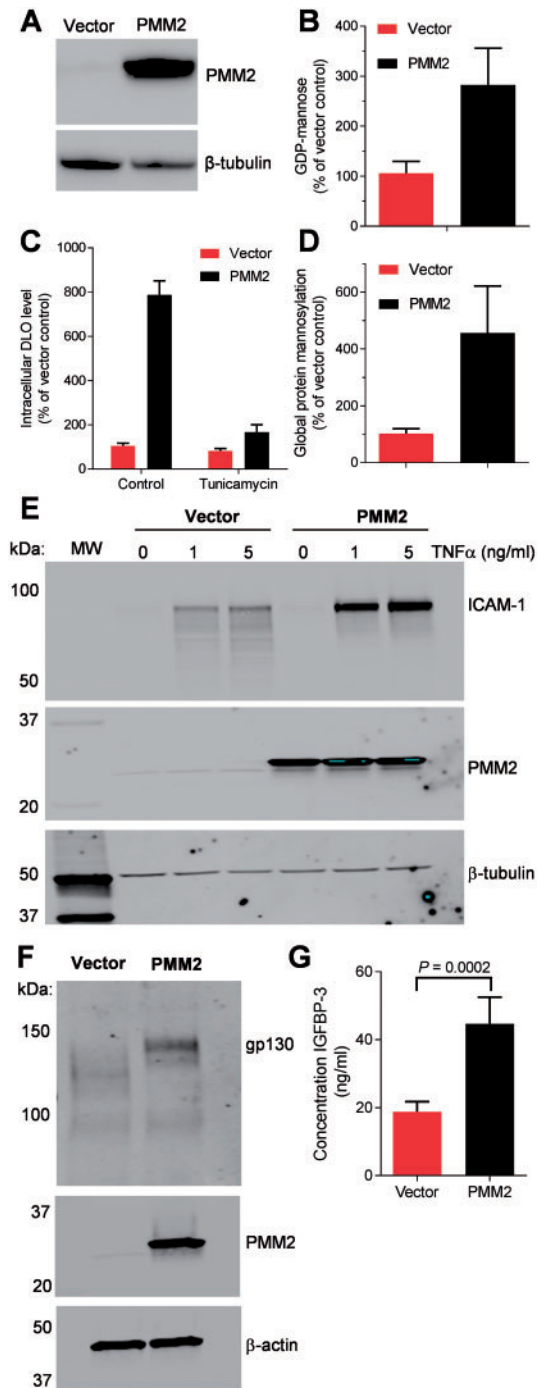


**Figure 6** WT-PMM2 over-expression restored PMM2 pathway activity and rescued expression of three endogenous glycoproteins in CDG-168 patient fibroblasts. (A) Western blot showing over-expression of human WT-PMM2 in CDG-168 cells. (B) GDP-mannose, (C) DLO and (D) global mannosylation levels were all elevated by WT-PMM2 over-expression (mean  $\pm$  SD from four independent experiments). For B and C, each experiment was repeated at least twice. Representative data from one experiment are shown as mean  $\pm$  SD from triplicate. (E) CDG-168 cells with and without WT-PMM2 over-expression were treated with TNF $\alpha$  at the indicated concentrations for 18 h, cell lysates were prepared and equal volumes of sample were probed for ICAM-1, PMM2 and  $\beta$ -tubulin (as a loading control) by western blotting. (F) CDG-168 cells with and without WT-PMM2 over-expression were probed for gp130, PMM2 and  $\beta$ -actin levels. (G) Human IGFBP-3 levels in cell culture supernatants were analyzed by ELISA, mean  $\pm$  SD, statistical significance tested with Student t-test. Representative data from three independent experiments are shown.

Patients with PMM2-CDG have not shown clinical improvement when given mannose supplements (37,38). In the present study, mannose supplementation did not improve survival of *Pmm2*<sup>R137H/F115L</sup> pups, but it did improve survival of *Pmm2*<sup>F115L/F115L</sup> homozygous pups. The mechanism is unknown, but it may involve substrate stabilization of the mutant PMM2 dimer interface or protection against thermal denaturation (39). Another possibility is that mannose supplementation increases mannose flux into the glycosylation pathway (22,40). Reducing MPI activity further enhances this flux by redirecting mannose from glycolysis toward glycosylation (35,41). Our preliminary (unpublished) results support this concept since mannose supplements (20 mg/ml mannose) rescue embryonic lethality of *Pmm2*<sup>R137H/F115L</sup> mutant mice only when they also carry an *Mpi*<sup>Y255C/Y255C</sup> mutation. These results encourage further exploration of the potential therapeutic value of increasing mannose flux toward glycosylation.

In summary, our study describes the first clinically relevant mouse model of PMM2-CDG. Viable mice with the patient-relevant genotype, *Pmm2*<sup>R137H/F115L</sup>, were generated. This allowed, for the first time, detailed postnatal phenotypic and molecular characterization of an *in vivo* PMM2-CDG disease model and indeed, this model recapitulated many human disease features. We also paired our mouse model with *in vitro* assays analyzing fibroblasts from patients with PMM2-CDG, and showed a high degree of correlation between the two systems. This validated model can now be used to assess future glycosylation-enhancing therapies with the potential to treat this disease.

## Materials and Methods

### Generation of *Pmm2*<sup>F115L</sup> and *Pmm2*<sup>R137H</sup> knock-in mice

The *Pmm2*<sup>F115L</sup> and *Pmm2*<sup>R137H</sup> knock-in targeting vectors were assembled using genomic fragments of the mouse *Pmm2* gene including a 3.0-kb 5' arm and a 7.6-kb 3' arm retrieved from 129S6/SvEv BAC DNA (OriGene Technologies) via an *Escherichia coli*-based chromosome engineering system (42), a *loxP*-flanked neomycin resistance cassette (*Neo*<sup>r</sup>) and a thymidine kinase (TK) gene, which served as negative selection for genomic integration. The 3' arm contained murine *Pmm2* exon 5 bearing the F115L or R137H mutations, which were created by PCR-based mutagenesis. The linearized targeting construct was electroporated into 129S6/SvEv mouse embryonic stem (ES) cells. Following homologous recombination in ES cells, an expression vector for Cre recombinase was transiently transfected to delete the *Neo*<sup>r</sup> cassette. Targeted ES cells were identified by PCR and sequencing analyses, and then injected into mouse blastocysts to produce chimeric mice. The chimeric mice were bred to C57BL/6J mice for germline transmission. Mice were genotyped using PCR primers spanning the position of the residual *loxP* site (5'-CCTCTGACATTTCTCCAACAAG-3' and 5'-GCGTAAGGCATGCGCCATCAC-3'), generating a 168-bp PCR product in WT mice and a 270-bp PCR product in knock-in mice. Initial litters were also analyzed for the presence of mutation by PCR and sequencing. All mutant animals were bred on a mixed 129 $\times$  C57BL/6J background.

Mice were bred and maintained in a barrier facility under pathogen-free conditions at WuXiAppTec (Shanghai, China). For mannose treatment studies, pregnant dams and pups were continuously supplied with 5 mM mannose in their drinking water. Mice were housed on 12 h/12 h light/dark cycle and given *ad libitum* access to food and water.

### Cell culture including MEF isolation and growth conditions

HFF-1 cells were from ATCC. PMM2-CDG patient-derived fibroblasts were isolated as described (43–46). HFF-1s and PMM2-CDG fibroblasts were cultured in Dulbecco's modified Eagle's medium (DMEM) (Invitrogen) supplemented with 30% fetal bovine serum (FBS) (Invitrogen). MEFs were harvested from embryos at 12.5 dpc. MEFs were cultured in DMEM (Invitrogen) supplemented with 10% FBS (Invitrogen), 2 mM GlutaMAX (Life Technologies), 100 units/ml penicillin and 100 µg/ml streptomycin, at 37 °C with 5% CO<sub>2</sub>.

### Mouse embryo fixation, staining and histology

For histological analysis, mouse embryos were harvested at different days of development. Whole embryos were fixed in 10% neutral-buffered formalin, embedded in paraffin, sectioned (3-µm thick) and stained with hematoxylin and eosin (H&E) according to standard laboratory protocols.

### Micro-CT imaging

Mice were anesthetized by 1% pentobarbital sodium (50 mg/kg, i.p.) for micro-CT scans with a GE eXplore Locus (GE Healthcare). All scans were performed in the same mode: 80 kV X-ray voltage, 450 µA current, 0.045 mm effective pixel size, 360° tomographic rotation and a rotation step of 0.9° with an exposure time of 400 ms for each view. All scans were reconstructed as 3D images by eXplore MicroView 2.0 analysis software with the same parameters.

### Western blotting of mouse plasma and cell culture samples

Mouse plasma samples were diluted 1:1000 in phosphate-buffered saline (PBS). Control BL/6 mouse plasma was either untreated (intact glycosylation) or deglycosylated with N-Glycanase (PROzyme) per the manufacturer's protocol. Cell lines were grown as indicated and lysed in equal volumes of RIPA lysis buffer (Boston Bioproducts) containing protease and phosphatase inhibitors (Roche). Briefly, 20 µl of each diluted plasma sample or equal amounts of cell culture extract was boiled for 10 min in 1× loading buffer (Boston Bioproducts). Samples were electrophoresed on a 4–15% gradient gel (Bio-Rad), transferred to nitrocellulose membranes (Invitrogen) and probed for antigens of interest. The following primary antibodies were used: anti-Transferrin (Abcam, ab82411); biotinylated anti-ALS (R&D Systems, BAF1436); anti-ICAM-1 (Santa Cruz Biotechnology, sc-8439); anti-GP130 (Cell Signaling Technology, CST-3732); anti-PMM2 (Abcam, ab138817); anti-β-actin (Cell Signaling Technology, CST-3700) and anti-β-tubulin (Cell Signaling Technology, CST-2128). Antigens were visualized using IRDye secondary antibodies and an Odyssey Imager (both LI-COR Biosciences).

### PMM-specific activity assay

Cells were assayed for total PMM-specific activity with a procedure adapted from a previous report (41). Cells were collected, washed in PBS, resuspended in 50 mM HEPES pH 7.4 and lysed by sonication. Cell extracts were cleared of debris by spinning at 14 000 rpm for 10 min and protein concentration was estimated

by the BCA method (Thermo Scientific). Reaction mixtures contained 60 µg of cellular protein (in a final volume of 135 µl per assay) in HEPES buffer, 30 µl of 7× enzyme mix (1.8 µl phosphoglucose isomerase, 1.6 µl of glucose-6-phosphate dehydrogenase, 11.4 µl mannose phosphate isomerase, 50 mM HEPES pH 7.4 to a final volume of 1000 µl), 30 µl of 7× chemical mix (1.35 mg NADP, 7.1 µl 4.9 M MgCl<sub>2</sub>, 150 µl of 100 µM glucose-1,6-bisphosphate, 50 mM HEPES pH 7.4 to a final volume of 1000 µl) and 15 µl of substrate (10 mM M1P). Samples were read at 340 nm every 2 min for 2–3 h.

### GDP-mannose quantification via LC-MS

Cells were plated at 2.5 × 10<sup>6</sup> cells per well in 6-well plates and grown overnight. The next day, cells were allowed to equilibrate for 1 h in basal labeling media [RPMI (Life Technologies) containing 3% dialyzed FBS and supplemented with non-essential amino acids and L-glutamine with no glucose or mannose]. Cells were then incubated in basal labeling media with or without 5 mM glucose for 4 h. Next, cells were promptly washed in ice-cold ammonium carbonate buffer (7.2 g/l, pH 7.4) and placed on dry ice. Metabolites were extracted with 80/20 methanol/water at –20 °C containing an internal standard, U-<sup>13</sup>C<sub>5</sub> U-<sup>15</sup>N<sub>1</sub> <sup>2</sup>H<sub>5</sub> glutamic acid. Samples were dried, sealed and stored at –80 °C until LC-MS analysis was performed.

GDP-mannose was quantified by coupling an ultra-performance LC (UPLC) column (Waters) with a Xevo TQ-S mass spectrometer. Separation was accomplished using reverse phase ion pairing chromatography, applying an Acquity UPLC HSS T3, 1.8 µm, 2.1 × 50 mm column (Waters). Mobile phase A consisted of 95/5 water/methanol plus 15 mM acetic acid, 10 mM tributylamine, pH 4.95, and phase B was methanol. A linear gradient was run at 0.4 ml/min unless otherwise noted: 0 min, 2% B; 1 min, 2% B; 5 min 60% B; 5.3 min 90% B, 0.3 ml/min; 5.5 min, 2% B, 0.375 ml/min; 6 min, 2% B; 7 min 2% B. The source parameters applied were: capillary voltage 3 kV, desolvation temperature 300 °C, desolvation gas 800 l/h. GDP-mannose was monitored in negative ionization mode, with the 604 → 442 transition, 24 V collision energy and cone voltage of 62. Quantitation was performed against an external calibration curve.

### Global protein mannosylation quantification

Cells were seeded at 3 × 10<sup>4</sup> cells per well in 96-well plates and grown overnight. The next day, cells were incubated with serum-free DMEM (Life Technologies) containing 0.5 g/l glucose, 20 µCi <sup>3</sup>H-mannose and 4 µCi <sup>35</sup>S-methionine for 8 h at 37 °C. Cells were harvested in 400 µl Tris-EDTA, 650 µl DMEM was added and the cells were spun at 3500 rpm for 10 min. Pellets were frozen at –20 °C overnight. The next day, cell pellets were resuspended in 100 µl 10 mM Tris-HCl pH 7.4 with 1% NP40. Next, 20 µl of each lysate was mixed with 5 µl BSA (10 mg/ml), 175 µl water and 200 µl TCA 20%, then placed on ice for 2 h. Samples were then centrifuged at 13 000 rpm for 20 min and the supernatant was discarded. The precipitate was resuspended in 50 µl of 0.2 N NaOH by pipetting, vortexing and then adding to 5 ml of scintillation fluid. Radioactivity was counted with the Beckman scintillation counter dual labeling program (channel 1 = 3H, channel 2 = 35S, channel 3 none) for 2 min. Final data were calculated as follows: <sup>35</sup>S = W2/0.632 and <sup>3</sup>H = W3-35S, where W = window.

## DLO determination

Cells were seeded at  $6 \times 10^4$  cells per well in 48-well plates and grown overnight. The next day, the cells were washed with PBS, and 200  $\mu$ l DMEM without glucose containing 4  $\mu$ Ci/ml [ $2\text{-}^3\text{H}$ ]-mannose was added and incubated at 37 °C for 1 h. The labeling medium was then removed and cells were washed with PBS. Cells were then trypsinized, transferred to the 96-well polypropylene cell culture plate and pelleted. Next, cells were lysed in 200  $\mu$ l chloroform:methanol (C:M, 2:1) and vortexed for 1 min. The mixture was then centrifuged at 13 000 rpm for 10 min and the C:M layer was removed. The extraction was repeated twice more with 200  $\mu$ l C:M (2:1) each. The final pellet was allowed to air dry, and 200  $\mu$ l water was then added. The samples were vortexed for 1 min, centrifuged as above and the water was removed. This step was repeated twice more. Samples were then extracted with 100  $\mu$ l chloroform:methanol:water (10:10:3) three times, incubated for 10 min and centrifuged for each extraction to ensure maximum recovery. Samples were next dried and 150  $\mu$ l of scintillation cocktail was added. Incorporation of  $^3\text{H}$ -mannose into DLO was measured by radioactivity and counted with a MicroBeta reader (Perkin Elmer). CellTiter-Glo (Promega) cell viability values were used to normalize each sample for the number of cells. Samples were split after trypsinizing and half tested with CTG, half extracted for DLO levels.

## ELISA assays

The following ELISA kits were used: mouse IGFBP-3 (R&D Systems, MGB300), mouse IGF-1 (R&D Systems, MG100), mouse antithrombin III (Abcam, ab10880), mouse PTX3 (R&D Systems, MPTX30), mouse IGFBP-1 (R&D Systems, DY1588-05) and human IGFBP-3 (R&D Systems, SGB300). All assays were run according to the manufacturer's protocol. In some cases, the standard curve was adjusted to include more low concentrations to increase confidence in dilute samples. For most kits, plasma samples were diluted 1:1000 in PBS and then final dilutions were prepared in the appropriate assay buffer. For PTX3, the samples were diluted 1:100 and then to 1:300 in appropriate buffer. For IGFBP-1, the WT/WT, F115L/WT and R137H/WT samples were diluted 1:100 and then to 1:200 in appropriate buffer.

## Lentiviral over-expression of WT-PMM2 in PMM2-CDG patient fibroblast cells

Lentiviruses directing over-expression of the cDNA for WT-PMM2 and empty lentiviral vectors were generated by transfecting 293T cells with PLVX-IRES-ELF1 $\alpha$ -NEO-based over-expression plasmids with packaging (psPAX2) and envelope (pCMV-VSVG) plasmids in low antibiotic growth media, alongside no vector cells to provide the selection resistance control. Twenty-four hours post-transfection, cells were exchanged into growth media. Viral supernatants were collected 48 and 72 h post-transfection and pooled for infection of target cells.

The desired cell lines were generated by seeding CDG-168 cells at a level giving 20–40% confluence 24 h later. Viral supernatants were then added to the cells and polybrene added to 8  $\mu$ g/ml, plates spun at 1200g for 60 min at 37 °C, and incubated overnight. The next day, the supernatant was replaced with growth media and cells selected with 200  $\mu$ g/ml Geneticin (Invitrogen).

## Statistics

P-values were generated using one-way ANOVA followed by Tukey post-hoc tests for multiple comparisons or chi-squared test, using Prism v.6 (GraphPad).

## Study approval

Mice were bred and maintained at WuXi AppTec. All animal work was performed in accordance with protocols approved by the WuXi AppTec Institutional Animal Care and Use Committee.

## Supplementary Material

Supplementary Material is available at HMG online.

## Acknowledgements

The authors would like to thank all Agios scientific advisors for their guidance, and especially Matthew Vander Heiden and Ralph DeBerardinis for their critical review of the manuscript, all the scientists at Agios for their technical assistance and helpful discussion and the Agios management team for their support. Christine Tomlins, PhD, of Excel Scientific Solutions, Horsham, UK, provided editorial assistance, funded by Agios Pharmaceuticals, Inc.

*Conflict of Interest statement.* B.C., M.C., G.A.S., G.H., J.P., Y.Ch., C.S., M.D., L.S., S.-S.M.S., and S.J. are employees of and have ownership interest in Agios Pharmaceuticals. All other authors have declared no conflicts of interest.

## Funding

This work was supported by Agios Pharmaceuticals, Inc., the Rocket Fund (to H.H.F.) and R01 DK99551 (to H.H.F.). Funding to pay the Open Access publication charges for this article was provided by Agios Pharmaceuticals Inc.

## References

- Freeze, H.H. and Schachter, H. (2009) Genetic disorders of glycosylation. In Varki, A., Cummings, R.D., Esko, J.D., Freeze, H.H., Stanley, P., Bertozzi, C.R., Hart, G.W. and Etzler, M.E. (eds), *Essentials of Glycobiology*. Cold Spring Harbor Laboratory Press, Cold Spring Harbor, NY, Chapter 42.
- Cylwi, B., Naklicki, M., Chrostek, L. and Gruszewska, E. (2013) Congenital disorders of glycosylation. Part I. Defects of protein N-glycosylation. *Acta Biochim. Pol.*, **20**, 151–161.
- Freeze, H.H. (2009) Towards a therapy for phosphomannomutase 2 deficiency, the defect in CDG-Ia patients. *Biochim. Biophys. Acta*, **1792**, 835–840.
- Jaeken, J., van Eijk, H.G., van der Heul, C., Corbeel, L., Eeckels, R. and Eggermont, E. (1984) Sialic acid-deficient serum and cerebrospinal fluid transferrin in a newly recognized genetic syndrome. *Clin. Chim. Acta*, **144**, 245–247.
- Sharma, V., Ichikawa, M. and Freeze, H.H. (2014) Mannose metabolism: More than meets the eye. *Biochem. Biophys. Res. Commun.*, **453**, 220–228.
- Coman, D., Irving, M., Kannu, P., Jaeken, J. and Savarirayan, R. (2008) The skeletal manifestations of the congenital disorders of glycosylation. *Clin. Genet.*, **73**, 507–515.
- Mohamed, M., Theodore, M., Claahsen-van der Grinten, H., van Herwaarden, A.E., Huijben, K., van Dongen, L.,

- Kouwenberg, D., Lefeber, D.J., Wevers, R.A. and Morava, E. (2012) Thyroid function in PMM2-CDG: diagnostic approach and proposed management. *Mol. Genet. Metab.*, **105**, 681–683.
8. Schade van Westrum, S.M., Nederkoorn, P.J., Schuurman, P.R., Vuulsa, T., Duran, M. and Poll-The, B.T. (2006) Skeletal dysplasia and myelopathy in congenital disorder of glycosylation type 1A. *J. Pediatr.*, **148**, 115–117.
  9. Sparks, S.E. and Krasnewich, D.M. (2015) PMM2-CDG (CDG-Ia). GeneReviews® [Internet]. <http://www.ncbi.nlm.nih.gov/books/NBK1110/>, last accessed 29 March 2016.
  10. Thompson, D.A., Lyons, R.J., Russell-Eggitt, I., Liasis, A., Jagle, H. and Grunewald, S. (2013) Retinal characteristics of the congenital disorder of glycosylation PMM2-CDG. *J. Inherit. Metab. Dis.*, **36**, 1039–1047.
  11. Thiel, C., Lubke, T., Matthijs, G., von Figura, K. and Körner, C. (2006) Targeted disruption of the mouse phosphomannomutase 2 gene causes early embryonic lethality. *Mol. Cell. Biol.*, **26**, 5615–5620.
  12. Schneider, A., Thiel, C., Rindermann, J., DeRossi, C., Popovici, D., Hoffmann, G.F., Gröne, H.J. and Körner, C. (2012) Successful prenatal mannose treatment for congenital disorder of glycosylation-Ia in mice. *Nat. Med.*, **18**, 71–73.
  13. Kjaergaard, S., Schwartz, M. and Skovby, F. (2001) Congenital disorder of glycosylation type Ia (CDG-Ia): phenotypic spectrum of the R141H/F119L genotype. *Arch. Dis. Child.*, **85**, 236–239.
  14. Kjaergaard, S., Skovby, F. and Schwartz, M. (1998) Absence of homozygosity for predominant mutations in PMM2 in Danish patients with carbohydrate-deficient glycoprotein syndrome type 1. *Eur. J. Hum. Genet.*, **6**, 331–336.
  15. Le Bizec, C., Vuillaumier-Barrot, S., Barnier, A., Dupré, T., Durand, G. and Seta, N. (2005) A new insight into PMM2 mutations in the French population. *Hum. Mutat.*, **25**, 504–505.
  16. Matthijs, G., Schollen, E., Van Schaftingen, E., Cassiman, J.J. and Jaeken, J. (1998) Lack of homozygotes for the most frequent disease allele in carbohydrate-deficient glycoprotein syndrome type 1A. *Am. J. Hum. Genet.*, **62**, 542–550.
  17. Perez, B., Briones, P., Quelhas, D., Artuch, R., Vega, A.I., Quintana, E., Gort, L., Ecay, M.J., Matthijs, G., Ugarte, M. et al. (2011) The molecular landscape of phosphomannomutase deficiency in Iberian peninsula: identification of 15 population-specific mutations. *JIMD Rep.*, **1**, 117–123.
  18. Schollen, E., Kjaergaard, S., Legius, E., Schwartz, M. and Matthijs, G. (2000) Lack of Hardy-Weinberg equilibrium for the most prevalent PMM2 mutation in CDG-Ia (congenital disorders of glycosylation type Ia). *Eur. J. Hum. Genet.*, **8**, 367–371.
  19. Miller, B.S., Khosravi, M.J., Patterson, M.C. and Conover, C.A. (2009) IGF system in children with congenital disorders of glycosylation. *Clin. Endocrinol. (Oxf)*, **70**, 892–897.
  20. Coman, D., McGill, J., MacDonald, R., Morris, D., Klingberg, S., Jaeken, J. and Appleton, D. (2007) Congenital disorder of glycosylation type 1a: three siblings with a mild neurological phenotype. *J. Clin. Neurosci.*, **14**, 668–672.
  21. Linssen, M., Mohamed, M., Wevers, R.A., Lefeber, D.J. and Morava, E. (2013) Thrombotic complications in patients with PMM2-CDG. *Mol. Genet. Metab.*, **109**, 107–111.
  22. Freeze, H.H. (2013) Understanding human glycosylation disorders: biochemistry leads the charge. *J. Biol. Chem.*, **288**, 6936–6945.
  23. Baxter, R.C. (2014) IGF binding proteins in cancer: mechanistic and clinical insights. *Nat. Rev. Cancer*, **14**, 329–341.
  24. Yamada, P.M., Mehta, H.H., Hwang, D., Roos, K.P., Hevener, A.L. and Lee, K.W. (2010) Evidence of a role for insulin-like growth factor binding protein (IGFBP)-3 in metabolic regulation. *Endocrinology*, **151**, 5741–5750.
  25. Waetzig, G.H., Chalaris, A., Rosenstiel, P., Suthaus, J., Holland, C., Karl, N., Vallés Uriarte, L., Till, A., Scheller, J., Gröttinger, J. et al. (2010) N-linked glycosylation is essential for the stability but not the signaling function of the interleukin-6 signal transducer glycoprotein 130. *J. Biol. Chem.*, **285**, 1781–1789.
  26. Panneerselvam, K. and Freeze, H.H. (1996) Mannose corrects altered N-glycosylation in carbohydrate-deficient glycoprotein syndrome fibroblasts. *J. Clin. Invest.*, **97**, 1478–1487.
  27. Kjaergaard, S., Skovby, F. and Schwartz, M. (1999) Carbohydrate-deficient glycoprotein syndrome type 1A: expression and characterisation of wild type and mutant PMM2 in *E. coli*. *Eur. J. Hum. Genet.*, **7**, 884–888.
  28. Grunewald, S. (2009) The clinical spectrum of phosphomannomutase 2 deficiency (CDG-Ia). *Biochim. Biophys. Acta*, **1792**, 827–834.
  29. Kjaergaard, S., Müller, J. and Skovby, F. (2002) Prepubertal growth in congenital disorder of glycosylation type Ia (CDG-Ia). *Arch. Dis. Child.*, **87**, 324–327.
  30. Inforzato, A., Doni, A., Barajon, I., Leone, R., Garlanda, C., Bottazzi, B. and Mantovani, A. (2013) PTX3 as a paradigm for the interaction of pentraxins with the complement system. *Semin. Immunol.*, **25**, 79–85.
  31. Guillard, M., Wada, Y., Hansikova, H., Yuasa, I., Vesela, K., Ondruskova, N., Kadoya, M., Janssen, A., Van den Heuvel, L.P., Morava, E. et al. (2011) Transferrin mutations at the glycosylation site complicate diagnosis of congenital disorders of glycosylation type I. *J. Inherit. Metab. Dis.*, **34**, 901–906.
  32. Marklova, E. and Albahri, Z. (2007) Screening and diagnosis of congenital disorders of glycosylation. *Clin. Chim. Acta*, **385**, 6–20.
  33. Yu, Y., Xu, J., Liu, Y. and Chen, Y. (2012) Quantification of human serum transferrin using liquid chromatography-tandem mass spectrometry based targeted proteomics. *J. Chromatogr. B. Analyt. Technol. Biomed. Life Sci.*, **902**, 10–15.
  34. Lacey, J.M., Bergen, H.R., Magera, M.J., Naylor, S. and O'Brien, J.F. (2001) Rapid determination of transferrin isoforms by immunoaffinity liquid chromatography and electrospray mass spectrometry. *Clin. Chem.*, **47**, 513–518.
  35. Sharma, V., Nayak, J., DeRossi, C., Charbono, A., Ichikawa, M., Ng, B.G., Grajales-Esquivel, E., Srivastava, A., Wang, L., He, P. et al. (2014) Mannose supplements induce embryonic lethality and blindness in phosphomannomutase isomerase hypomorphic mice. *FASEB J.*, **28**, 1854–1869.
  36. Hammacher, A., Richardson, R.T., Layton, J.E., Smith, D.K., Angus, L.J., Hilton, D.J., Nicola, N.A., Wijdenes, J. and Simpson, R.J. (1998) The immunoglobulin-like module of gp130 is required for signaling by interleukin-6, but not by leukemia inhibitory factor. *J. Biol. Chem.*, **273**, 22701–22707.
  37. Kjaergaard, S., Kristiansson, B., Stibler, H., Freeze, H.H., Schwartz, M., Martinsson, T. and Skovby, F. (1998) Failure of short-term mannose therapy of patients with carbohydrate-deficient glycoprotein syndrome type 1A. *Acta Paediatr.*, **87**, 884–888.
  38. Mayatepek, E., Schroder, M., Kohlmuller, D., Bieger, W.P. and Nutzenadel, W. (1997) Continuous mannose infusion in carbohydrate-deficient glycoprotein syndrome type I. *Acta Paediatr.*, **86**, 1138–1140.
  39. Andreotti, G., Pedone, E., Giordano, A. and Cubellis, M.V. (2013) Biochemical phenotype of a common disease-causing mutation and a possible therapeutic approach for the

- phosphomannomutase 2-associated disorder of glycosylation. *Mol. Genet. Genomic Med.*, **1**, 32–44.
40. Ichikawa, M., Scott, D.A., Losfeld, M.E. and Freeze, H.H. (2014) The metabolic origins of mannose in glycoproteins. *J. Biol. Chem.*, **289**, 6751–6761.
  41. Sharma, V., Ichikawa, M., He, P., Scott, D.A., Bravo, Y., Dahl, R., Ng, B.G., Cosford, N.D. and Freeze, H.H. (2011) Phosphomannose isomerase inhibitors improve N-glycosylation in selected phosphomannomutase-deficient fibroblasts. *J. Biol. Chem.*, **286**, 39431–39438.
  42. Lee, E.C., Yu, D., Martinez de Velasco, J., Tessarollo, L., Swing, D.A., Court, D.L., Jenkins, N.A. and Copeland, N.G. (2001) A highly efficient *Escherichia coli*-based chromosome engineering system adapted for recombinogenic targeting and subcloning of BAC DNA. *Genomics*, **73**, 56–65.
  43. Enns, G.M., Steiner, R.D., Buist, N., Cowan, C., Leppig, K.A., McCracken, M.F., Westphal, V., Freeze, H.H., O'Brien, J. F., Jaeken, J. et al. (2002) Clinical and molecular features of congenital disorder of glycosylation in patients with type 1 sialotransferrin pattern and diverse ethnic origins. *J. Pediatr.*, **141**, 695–700.
  44. Krasnewich, D., O'Brien, K. and Sparks, S. (2007) Clinical features in adults with congenital disorders of glycosylation type Ia (CDG-Ia). *Am. J. Med. Genet. C Semin. Med. Genet.*, **145C**, 302–306.
  45. Matthijs, G., Schollen, E., Bjursell, C., Erlandson, A., Freeze, H., Imtiaz, F., Kjaergaard, S., Martinsson, T., Schwartz, M., Seta, N. et al. (2000) Mutations in PMM2 that cause congenital disorders of glycosylation, type Ia (CDG-Ia). *Hum. Mutat.*, **16**, 386–394.
  46. Westphal, V., Peterson, S., Patterson, M., Tournay, A., Blumenthal, A., Treacy, E.P. and Freeze, H.H. (2001) Functional significance of PMM2 mutations in mildly affected patients with congenital disorders of glycosylation Ia. *Genet. Med.*, **3**, 393–398.